



Influences of aerosol physiochemical properties and new particle formation on CCN activity from observation at a suburban site of China



Yanan Li ^{a,b}, Fang Zhang ^{a,*}, Zhanqing Li ^{a,c,**}, Li Sun ^d, Zhenzhu Wang ^e, Ping Li ^a, Yele Sun ^f, Jingye Ren ^a, Yuying Wang ^a, Maureen Cribb ^c, Cheng Yuan ^g

^a College of Global Change and Earth System Science, Beijing Normal University, Beijing 100875, China

^b CMA Meteorological Observation Center, Centre for Atmosphere Watch and Services, Beijing 100081, China

^c Earth System Science Interdisciplinary Center and Department of Atmospheric and Oceanic Science, University of Maryland, College Park, MD, USA

^d Weather Modification Office in Liaoning Province, Shenyang 110166, China

^e Key Laboratory of Atmospheric Composition and Optical Radiation, Anhui Institute of Optics and Fine Mechanics, Chinese Academy of Sciences, Hefei 230031, China

^f State Key Laboratory of Atmospheric Boundary Layer Physics and Atmospheric Chemistry, Institute of Atmospheric Physics, Chinese Academy of Sciences, Beijing 100029, China

^g School of Atmospheric Sciences, Nanjing University, Nanjing 210023, China

ARTICLE INFO

Article history:

Received 16 August 2016

Received in revised form 18 January 2017

Accepted 18 January 2017

Available online 19 January 2017

Keywords:

Cloud condensation nuclei

Diurnal variation

Activation ratio

Closure study

New particle formation

ABSTRACT

With the aim of understanding the impact of aerosol particle size and chemical composition on CCN activity, the size-resolved cloud condensation nuclei (CCN) number concentration (N_{CCN}), particle number size distribution (PSD) (10–600 nm), and bulk chemical composition of particles with a diameter $< 1.0 \mu\text{m}$ (PM_{10}) were measured simultaneously at Xinzhou, a suburban site in northern China, from 22 July to 26 August 2014. The N_{CCN} was measured at five different supersaturations (SS) ranging from 0.075%–0.76%. Diurnal variations in the aerosol number concentration (N_{CN}), N_{CCN} , the bulk aerosol activation ratio (AR), the hygroscopicity parameter (K_{chem}), and the ratio of 44 mass to charge ration (m/z 44) to total organic signal in the component spectrum (f_{44}), and the PSD were examined integrally to study the influence of particle size and chemical composition on CCN activation. We found that particle size was more related to the CCN activation ratios in the morning, whereas in the afternoon (~ 1400 LST), K_{chem} and f_{44} were more closely associated with the bulk AR. Assuming the internal mixing of aerosol particles, N_{CCN} was estimated using the bulk chemical composition and real-time PSD. We found that the predicted CCN number concentrations were underestimated by 20–30% at SS $< 0.2\%$ probably due to the measurement uncertainties. Estimates were more accurate at higher SS levels, suggesting that the hygroscopicity parameter based on bulk chemical composition information can provide a good estimate of CCN number concentrations. We studied the impacts of new particle formation (NPF) events on size-resolved CCN activity at the “growth” stage and “leveling-off” stage during a typical NPF event by comparing with the case during non-NPF event. It has been found that CCN activation was restrained at the “growth” stage during which larger particle diameters were needed to reach an activation diameter (D_a), and the bulk AR decreased as well. However, during the “leveling-off” stage, a lower D_a was observed and CCN activation was greatly enhanced.

© 2017 Elsevier B.V. All rights reserved.

1. Introduction

As a subset of atmospheric aerosols, cloud condensation nuclei (CCN) enable the condensation of water vapor and the formation of cloud droplets. When the water vapor content of a cloud remains constant, elevated CCN number concentrations increases the number of cloud droplets but decreases their sizes. This changes the cloud albedo

(Twomey, 1977), the cloud life span (Albrecht, 1989), cloud microphysical properties, and ultimately, climate. Evaluating the interaction between aerosol particles and clouds is one of the largest uncertainties in the quantification of aerosol effects on climate (IPCC, 2013; Chin et al., 2009) with CCN at the heart of the problem (Medina et al., 2007). Modelers have simulated the global spatial distribution of CCN concentration (Lee et al., 2012), but with large uncertainty. Thus, obtaining an accurate temporal and spatial CCN number distribution is an important and challenging issue. Many ground-based CCN observation field campaigns have been performed at different sites with different surface types around the world, such as those on mountains (DeFelice and Saxena, 1994; Miao et al., 2015), in forests (Gunthe et al., 2009), on plains (Rissman et al., 2006; Deng et al., 2011, 2013),

* Corresponding author.

** Correspondence to: Z. Li, Earth System Science Interdisciplinary Center and Department of Atmospheric and Oceanic Science, University of Maryland, College Park, MD, USA.

E-mail addresses: fang.zhang@bnu.edu.cn (F. Zhang), zli@atmos.umd.edu (Z. Li).

over oceans (Yum and James, 2004) and in megacities (Almeida et al., 2014; Leng et al., 2014a, 2014b). Owing to the complicated properties and short life span of aerosols, CCN characteristics can fluctuate over time at a fixed site (e.g. Almeida et al., 2014; Zhang et al., 2014), while direct long-term measurements of CCN number concentrations on a global scale is likely unrealistic. It is key to understand what controls the ability of aerosols to act as CCN and to develop typical CCN parameterization schemes for use in models. Aerosol activation depends on the aerosol mixing state, size distribution and chemical composition, however, there is no consensus as to how accurate is the measurement for each of these factors is needed to predict CCN number concentrations (Dusek et al., 2006; Rissman et al., 2006; McFiggans et al., 2006; Anttila and Kerminen, 2007; Hudson, 2007; Quinn et al., 2008; Zhang et al., 2012; Ma et al., 2013). Aerosol-CCN closure study, or comparing predicted CCN concentrations with measurements based on Köhler theory, is a valid approach to test the relative significance of aerosol physical and chemical characteristics. It can also help to form a framework for predicting N_{CCN} .

New particle formation (NPF), recognized as contributing toward 40%–55% of the total aerosol number concentration (Yu et al., 2008), was observed to enhance N_{CCN} in both a relatively clean environment (O'Dowd, 2001; Sihto et al., 2011; Kalkavouras et al., 2017) and at polluted sites (Wiedensohler et al., 2009; Yue et al., 2011; Ma et al., 2016). For example, Kuang et al. (2009) developed a semi-analytical model for CCN prediction by simulating the growth of a subset of an aerosol population from 3 to 100 nm and found that the NPF enhanced CCN number concentrations by a mean factor of 3.8. Asmi et al. (2011) assumed that particles with sizes larger than 80 nm would activate into CCN. On average, NPF increased CCN number concentrations by a factor of 2.11 ± 1.14 . To our knowledge, most of the previous studies have not yet investigated the impacts on size-resolved CCN activation ratio as well as changes in critical diameter during NPF events. The goal of our research is to investigate the variation in the critical diameter of particles in an NPF case against that in a background case using size-resolved CCN observations in an attempt to study the influence of NPF on CCN activity. In particular, we will focus on the “growth” stage and the “leveling-off” stage of the NPF to investigate the effect with the aim of improving the parameterization of CCN in climate models.

In China, the high number concentration and complex properties of aerosols from both the ground and vertical profile measurements (Li et al., 2007; Li et al., 2015) increases the variability in cloud droplet

formation, which has a profound effect on climate change. Supported by the National Project “Observation and Modelling Study of Cloud, Aerosol and their Climate Effect”, we conducted a field campaign called “Atmosphere, Aerosol, Cloud and CCN” (A^2C^2) from 22 July to 26 August 2014 in northern China, which aimed to understand the impact of aerosol particle size and chemical composition on CCN activity. In the paper, Section 2 describes the observation site and data used in the study. Section 3 describes the theory and methods, including derivations of the hygroscopic parameter and critical diameter (D_{crit}). Section 4 presents the overall characteristics of aerosols, CCN number concentrations, aerosol activation, the CCN closure study using bulk chemical composition information and the impact of NPF on CCN activity. Conclusions were summarized in the last section.

2. Observation site and measurements

2.1. Observation site

The observation site, Xinzhou (38.24°N, 112.43°E; 1500 m asl XZ), is located on the border of the Loess Plateau and the Northern China Plain, about 78 km northwest of Taiyuan (Fig. 1). The site experiences a warm temperate continental monsoon climate. During the observation period, the Xinzhou site was surrounded by fields of corn plants. In summer, the dominant winds come from the northeast and southwest. The SMPS combined with the DMT CCN-100 was set during the campaign from 22 July to 26 August 2014. Details about the site information and measurement can also be found in Zhang et al. (2016).

2.2. Measurements

The instruments were housed in a $2 \times 6 \times 2$ m container, surrounded by corn plant fields. The automatic meteorological station that measured the ambient temperature, relative humidity, rain rate, wind speed, and wind direction was about 20 m away from the container. Atmospheric aerosol particles were collected from a sampling inlet that was installed ~1.5 m above the roof of the container, then passed through a silica gel desiccant drying tube, which assured that the relative humidity level was below 30% (Leng et al., 2013), before entering into a TSI Scanning Mobility Particle Sizer (SMPS). The SMPS is comprised of a 3080 electric classifier, a 3022A condensation particle counter (CPC), and a microcomputer. The particle number size distribution

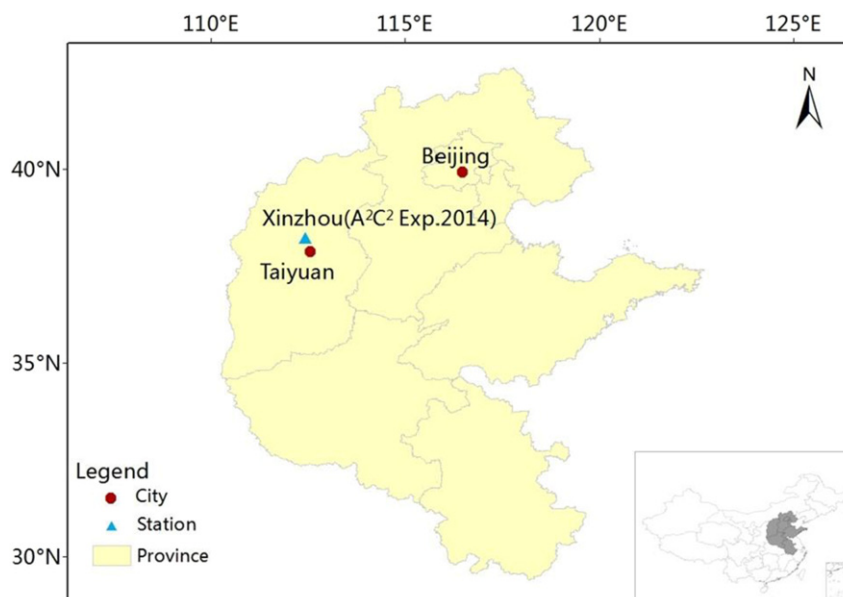


Fig. 1. Geographic locations of Xinzhou site.

for the mobility diameter was between 10 and 600 nm. Because we measured the size-resolved CCN number concentrations, which are with the particle size range of 10–600 nm and the large particles were included here. Therefore, without considering of the large particles will not cause an uncertainty in CCN closure study. A set of particle number size distributions was obtained every 255 s: 240 s for the voltage upscan time and 15 s retrace time. A Droplet Measurement Technology Cloud Condensation Nuclei counter (CCNc; Roberts and Nenes, 2006) was situated downstream of the SMPS. The whole experimental set-up and method is also described as Scanning Mobility CCN Analysis (SMCA), introduced by Moore et al. (2010). The atmospheric aerosol flow streaming out of the differential mobility analyzer (DMA), which is a basic part the electric classifier, at a rate of 0.8 l per minute (lpm) was split, going into the CPC at a flowrate of 0.3 lpm and into the CCNc with a sheath-to-sample flowrate ratio of 10. Five SS (0.07%, 0.1%, 0.2%, 0.4%, and 0.8%, each running for 10 min), were set in the CCNc and corrected to 0.075%, 0.13%, 0.17%, 0.39%, and 0.76% after being calibrated with pure ammonium sulfate following the procedures described by Rose et al. (2008). Thus, two sets of particle number size distribution for each SS were obtained. The first five minutes of data were removed to exclude the influence of the transition in SS according to Deng et al. (2011). The fluctuation (relative standard deviation) for the second five minutes bulk CCN data is <3%. The SMPS and CCNc data were processed with multiple corrections following the method developed by Deng et al. (2011).

Black carbon (BC) was measured with a 7-wavelength online aethalometer (AE-31, Magee Scientific), whose flowrate setting was 5 lpm. The time resolution of BC data was 5 min. By comparing the difference between light transmission through the particle-laden sample spot and the particle-free reference spot in the filter, the BC concentration can be obtained (Cheng et al., 2006; Dumka et al., 2010).

The bulk chemical composition of particles with a diameter <1.0 μm (PM_{10}) was measured with an Aerodyne Aerosol Chemical Speciation Monitor (ACSM) at a time resolution of ~ 7.5 min. By this technique, the non-refractory submicron aerosol species including organics, sulfate, nitrate, ammonium, and chloride was measured simultaneously with the CCN measurement. Before sampling into the ACSM, aerosol particles were dried using a silica gel desiccant. The ACSM was operated with a scan rate of mass spectrometer at 500 ms amu^{-1} from m/z 10 to 150. f_{44} is calculated by the mass signal at m/z 44, which refers to the fraction of mass signal at m/z 44 in total organics. Higher f_{44} in organics indicates the particles being more oxidized. Regarding the calibration of the ACSM, mono-dispersed, size-selected 300 nm ammonium nitrate

particles within a range of concentrations were sampled into both the ACSM and a condensation particle counter (CPC). The ionization efficiency (IE) was then determined by comparing the response factors of the ACSM to the mass calculated with known particle size and number concentrations from the CPC. A collection efficiency factor of 0.5 was applied to account for the incomplete detection of particles primarily due to particle bounce effect, and was found to be appropriate for this site. A comparison of particle mass concentration from the ACSM with the integrated mass concentration from the SMPS was also made. The number concentrations measured by the SMPS were converted to the mass concentrations using chemically-resolved particle density that was estimated from the chemical composition of PM_{10} . The result showed that the PM_{10} (total mass of non-refractory and black carbon) from ACSM was well correlated with that of SMPS (with $r^2 = 0.65$), and the mass ratio of SMPS to ACSM is 0.62. A more detailed diagnostics of CE and the inter-comparison with SMPS measurements is given in Wang et al. (2016). And more detailed description of the operation and calibration of the ACSM are given by Ng et al. (2011) and Sun et al. (2012). In this study, the refractory components of aerosol include such as black carbon and dust. For black carbon, it accounts for about 2.4% of total PM_{10} ; for dust, because of their large size (usually in coarse mode) and thus is not within the detect range of the ACSM technique.

3. Derivation of hygroscopic parameter κ_{chem} and critical dry diameter D_{crit}

In this study, we calculated κ_{chem} based on bulk chemical composition observations during the field campaign. Assuming an internal mixture of chemical species as measured by the ACSM, the hygroscopic parameter κ_{chem} was derived according to the equation, $K = \sum_i \varepsilon_i \kappa_i$, where ε_i and κ_i are the volume fraction and hygroscopic parameter, respectively, of the i th species (Petters and Kreidenweis, 2007).

According to ACSM measurements, chemical composition constituents at the Xinzhou site were mainly organics, sulfate, and nitrate. The volume fraction of chloride and BC was <5%. Therefore, the particle hygroscopic parameter is (Petters and Kreidenweis, 2007):

$$\kappa_{chem} = \kappa_{Org} \varepsilon_{Org} + \kappa_{(\text{NH}_4)_2\text{SO}_4} \varepsilon_{(\text{NH}_4)_2\text{SO}_4} + \kappa_{\text{NH}_4\text{NO}_3} \varepsilon_{\text{NH}_4\text{NO}_3}$$

The hygroscopicity parameters for $(\text{NH}_4)_2\text{SO}_4$ and NH_4NO_3 are 0.61 and 0.67 (Petters and Kreidenweis, 2007). The value of κ_{Org} during the

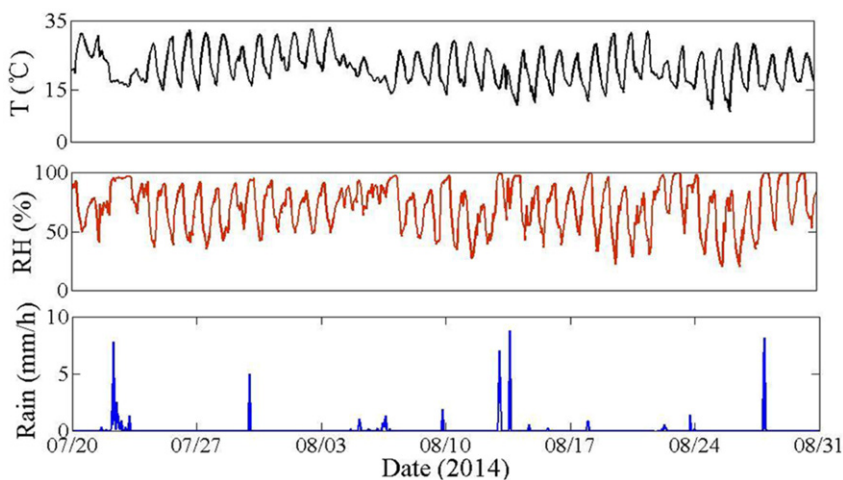


Fig. 2. Time series of meteorological parameters. The upper panel shows 24-h average temperature (T), the middle panel shows 24-h average relative humidity (RH), and the third panel shows the rain rate. The time period is 20 July to 31 August 2014.

field campaign can be estimated as: $\kappa_{org} = 2.10 \times f_{44} - 0.11$, where f_{44} is the fraction of m/z 44 in total organics (Mei et al., 2013). The volume fraction of each chemical species was obtained by dividing its mass concentration by its density. The densities of organics, $(\text{NH}_4)_2\text{SO}_4$, and NH_4NO_3 used in this work are 1200 kg m^{-3} (Turpin and Lim, 2001), 1770 kg m^{-3} and 1720 kg m^{-3} (Larson et al., 1988), respectively. The mean chemical composition derived κ_{chem} value during the entire period was 0.42 ± 0.04 . This value is higher than the global mean κ value for continental regions (0.27 ± 0.21) and much lower than that for marine regions (0.72 ± 0.24) (Andreae and Rosenfeld, 2008; Pringle et al., 2010).

Then we retrieved the critical diameter (D_{crit}) based on a κ -Köhler equation (Petters and Kreidenweis, 2007), which is described as,

$$S = \left(1 + \kappa \frac{D_0^3}{D^3 - D_0^3} \right)^{-1} \exp\left(\frac{4\sigma M_w}{RT\rho_w D}\right),$$

where κ is hygroscopic parameter, which is defined through its effect on the water activity of the solution; S is the supersaturation, D is the droplet diameter under different S , D_0 is the dry diameter of the particle, M_w is the molecular weight of water, σ is the surface tension of pure water,

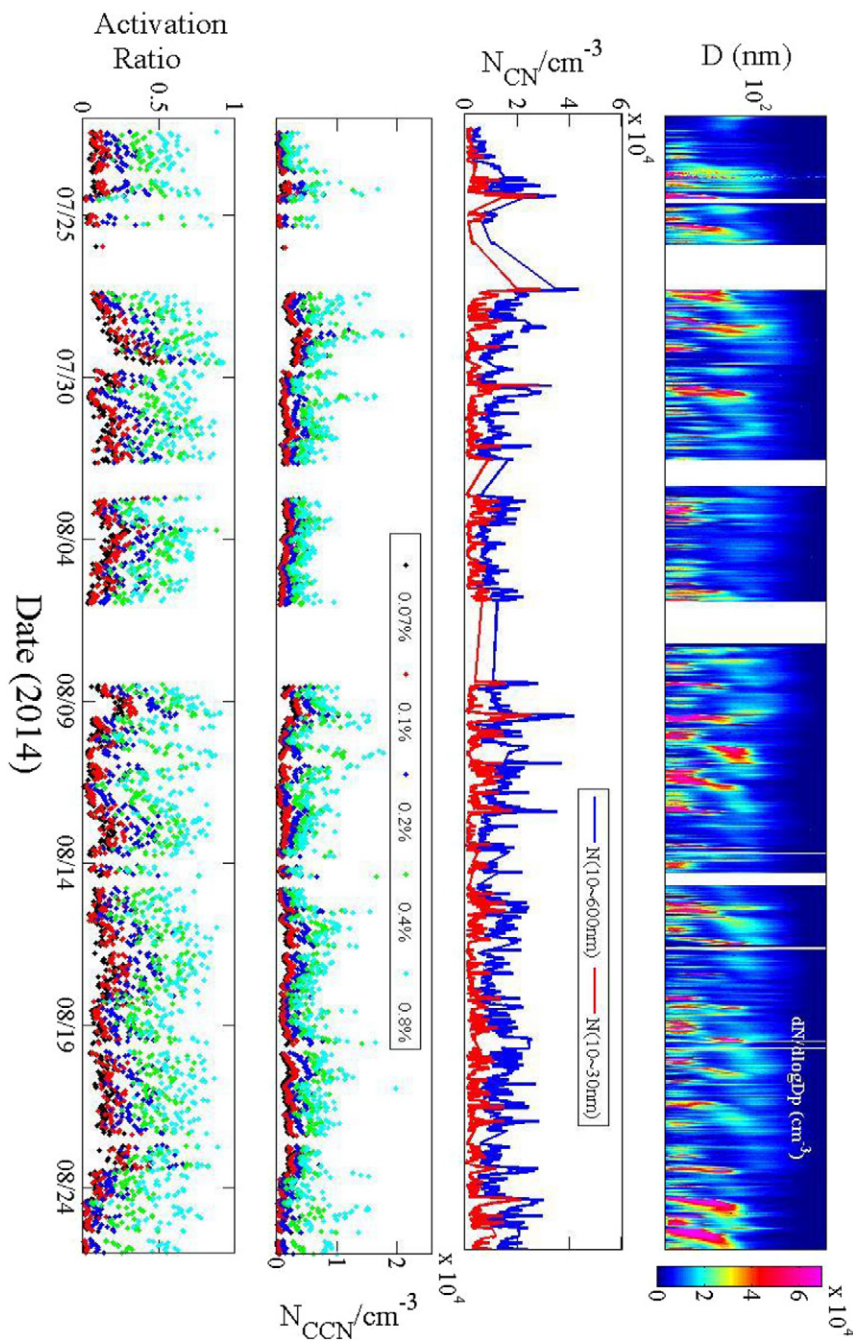


Fig. 3. From top to bottom: time series of the aerosol particle number size distribution; integral(10–600 nm, blue curve) and nucleation-mode (10–30 nm, red curve) CN number concentrations; CCN number concentrations at supersaturations of 0.075% (black dots), 0.13% (red dots), 0.17% (blue dots), 0.39% (green dots), and 0.76% (cyan dots); bulk CCN activation ratios at supersaturations of 0.075% (black dots), 0.13% (red dots), 0.17% (blue dots), 0.39% (green dots), and 0.76% (cyan dots). The time period is 22 July to 26 August 2014.

ρ_w is the density of water, R is the gas constant, and T is the absolute temperature.

When $\kappa > 0.2$, it can be calculated from the following approximate expression:

$$\kappa = \frac{4A^3}{27D^3 \ln^2 S}$$

$$A = \frac{4\sigma M_w}{RT\rho_w}$$

Here the κ equal to κ_{chem} , we thus calculated the critical dry diameter (D_{crit}). The D_{crit} of a particle with properties (SS, κ_{chem}) corresponds to the minimum value of D needed for the particle to be activated. Particles with sizes larger than D_{crit} will be activated.

4. Results

4.1. Overview of meteorological parameters, aerosol and CCN number concentrations during the field campaign

During the observation period, the average temperature was 21.6 °C and the average ambient relative humidity was 72.3%. Fig. 2 shows that surface temperature and relative humidity have opposite trends. Five short-term precipitation events occurred during the field campaign. The largest rain rate was $< 10 \text{ mm h}^{-1}$. When it rained, aerosol number concentrations dropped sharply. The dominant winds at Xinzhou were from the northeast and southwest during the field campaign.

Clear days were common at Xinzhou with many episodes of gas-to-particle formation (Shen et al., 2011). An NPF event was identified if (1) there was a sudden burst of nucleation mode particles and (2) the formation of nucleation mode particles lasted for several hours with a

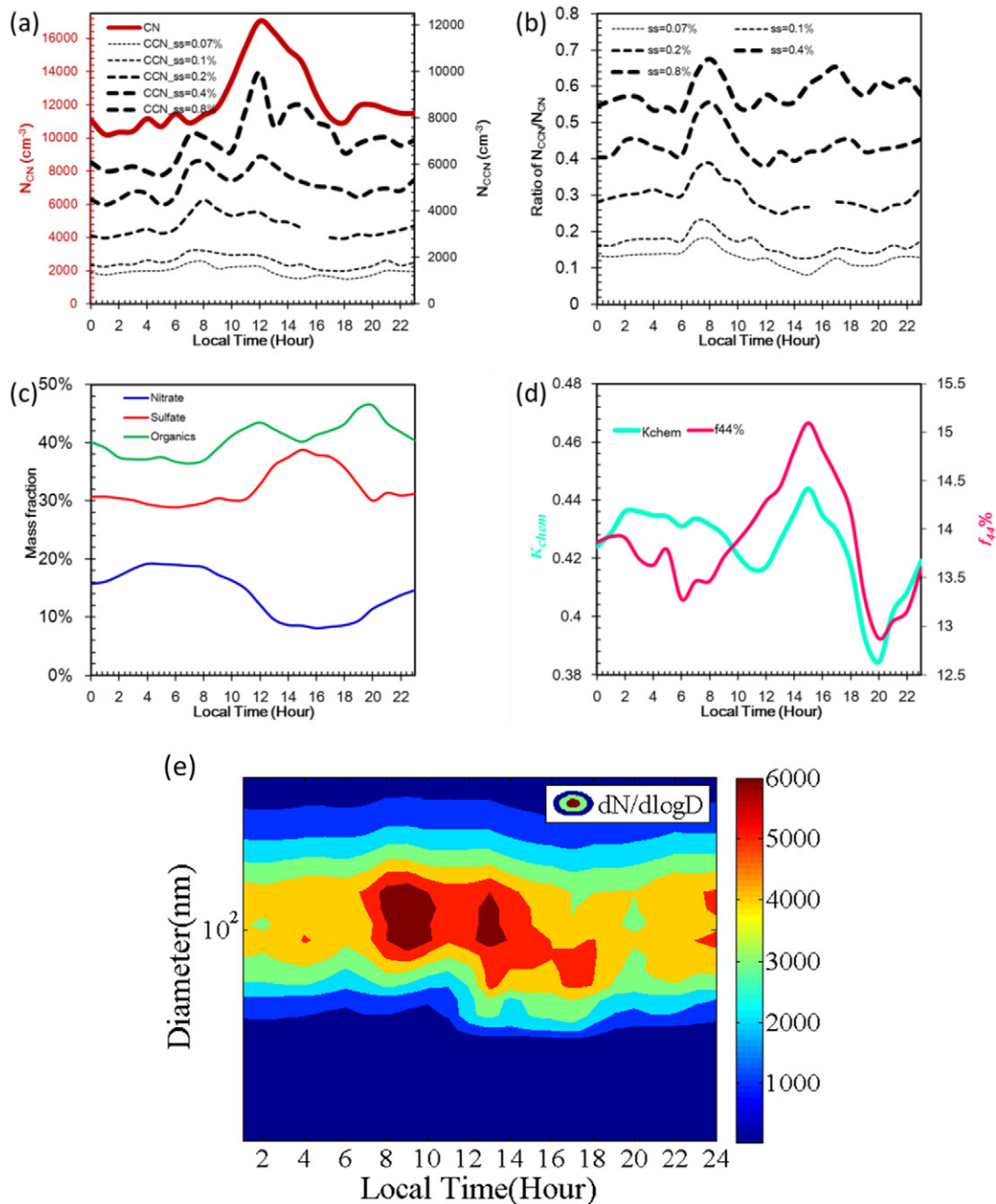


Fig. 4. Diurnal variations in (a) aerosol (CN) and CCN number concentrations, (b) the ratio of N_{CN} to N_{CCN} , (c) mass fractions of nitrate, sulfate, and organics, (d) κ_{chem} and f_{44} , and (e) the particle number size distribution.

subsequent growth in mean particle size (Birmili and Wiedensohler, 2000; Dal Maso et al., 2005; Vakkari et al., 2011; Kulmala et al., 2012). The significant growth to larger particles, which appears as a “banana” shape in the particle number size distribution and is representative of a NPF event (Shi et al., 2001; Heintzenberg et al., 2007; Olofson et al., 2009; Wang et al., 2013), was only observed on a few days. Most of the cases merely showed a sudden increase in aerosol number concentration but without growing to larger particles (Fig. 3, the first panel from the top), which we call non-typical NPF. The particle size diameter (D) corresponding to the maximum $dN/d\log D$ is ~ 100 nm, of which 60% of particles were in the nucleation mode.

According to Fig. 3 (the second and third panel from the top), both the aerosol and CCN number concentrations fluctuated largely during the observation period. The average aerosol number concentration is $12,195 \pm 5657 \text{ cm}^{-3}$, among which particles with D ranging from 10 to 30 nm accounted for 32.7% of all particles. Measured mean CCN number concentrations are $1353 \pm 777 \text{ cm}^{-3}$, $1769 \pm 974 \text{ cm}^{-3}$, $3264 \pm 1599 \text{ cm}^{-3}$, $5057 \pm 2325 \text{ cm}^{-3}$, $6920 \pm 3303 \text{ cm}^{-3}$ at SS of 0.075%, 0.13%, 0.17%, 0.39%, and 0.76%, respectively. Both the mean values and standard deviations increased with increasing SS. According to last panel in Fig. 3, the average bulk activation ratio, the ratio of N_{CCN} to N_{CN} , increased with increasing SS, i.e., $12.6 \pm 8\%$, $16.4 \pm 9\%$, $29.4 \pm 13\%$, $43.7 \pm 15\%$, and $58.1 \pm 15\%$ at SS of 0.075%, 0.13%, 0.17%, 0.39%, and 0.76%, respectively.

4.2. Diurnal variations

To investigate the influence of particle size and chemical composition on CCN activation, diurnal variations in N_{CN} , N_{CCN} , bulk AR, κ_{chem} , f_{44} , and the particle number size distribution over all days were examined (Fig. 4). Here, the f_{44} refers to the fraction of total organic mass signal at m/z 44. The m/z 44 signal is mostly due to acids or acid-derived species, such as esters, and f_{44} is closely related to the organic oxidation level, i.e., O:C ratio. Oxidized/aged acids are generally more hygroscopic and easily activated. Both CN and CCN number concentrations peaked

around 1200 LT (Fig. 4a). And the enhancement in bulk AR after 1200 LT was observed at higher SS because most of the particles were nucleation-mode particles, which were difficult to activate at lower SS (Fig. 4b). We examined jointly the changes in chemical composition (Fig. 4c) and size distribution (Fig. 4e), which showed that the increase in bulk AR until 1600 LT is largely attributed to the increase in sulfate and aged/oxidized organics. From 1200 to 1600 LT, the κ_{chem} and f_{44} increased simultaneously in Fig. 4d, while number concentration of accumulation-mode particles decreased.

Another peak in CCN number concentration and the bulk AR is seen from 0700 to 0800 LT. During this time, the mass fractions of nitrate, sulfate, and organics were all at a relatively stable level, but the number concentrations of aerosol particles with $D > 100$ nm increased significantly and the particle size showed a slight increasing trend (Fig. 4e). This means that the particle size took on a dominant role in controlling aerosol activity from 0700 to 0800 LT. Our analysis shows the integral effect of aerosol size and chemical composition on CCN activity over the entire period.

4.3. CCN closure study

Assuming internal mixing, a homogenous composition of the particles as provided by the ACSM, and simplified Köhler theory, we calculated the critical dry diameter (D_{crit}). The D_{crit} of a particle with properties (SS, κ_{chem}) corresponds to the minimum value of D needed for the particle to be activated. Particles with sizes larger than D_{crit} will be activated. The predicted total CCN number concentration (CCN_Predicted) is obtained from the step-wise integration of the particle number size distribution (PSD) from D_{crit} to 600 nm, as 600 nm is the largest diameter in the processed data observed at the Xinzhou site. The time resolution of κ_{chem} derived from the ACSM is about 7.5 min and the time resolution of size-resolved CCN measurements is ~ 10 min. We assume that these two sets of measurements are simultaneous measurements if their drift time is within 5 min. Comparisons of predicted and measured N_{CCN} estimated using the derived D_{crit} for different SS levels are shown in Fig. 5.

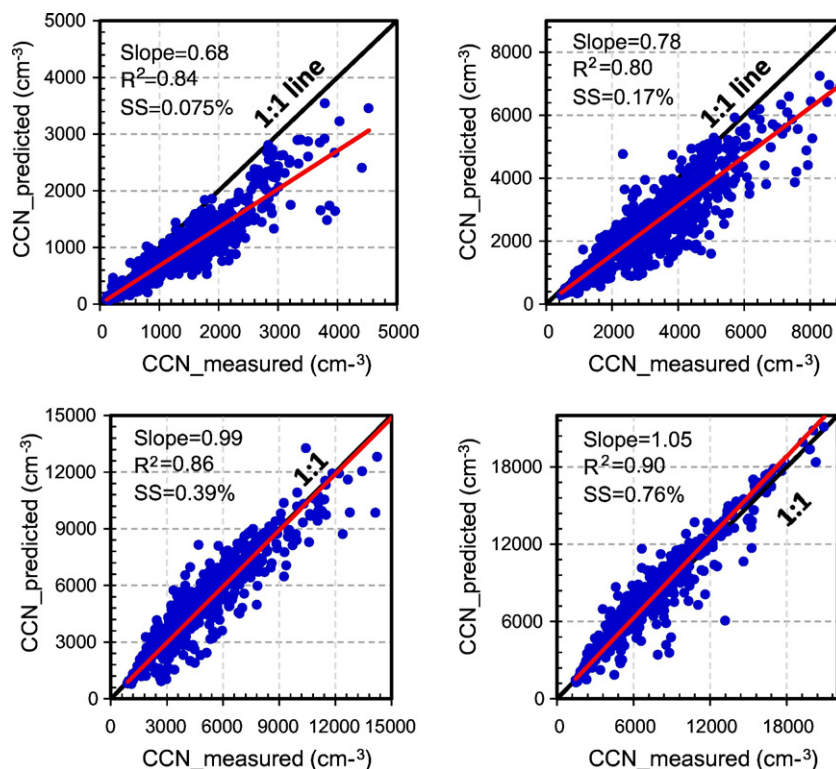


Fig. 5. Comparison of predicted and measured N_{CCN} estimated using the derived D_{crit} for different supersaturation levels. Black lines represent the 1:1 line and red lines represent the linear best-fit lines.

Measured and predicted N_{CCN} at the different SS levels are moderately correlated ($R^2 = 0.8–0.9$). N_{CCN} was largely underestimated at SS equal to 0.075% and 0.17% (by 32% and 22%, respectively). The underestimation decreased as SS increased. The best agreement between predicted and observed N_{CCN} is seen when $SS = 0.39\%$ (the slope and R^2 are 0.99 and 0.86, respectively). At $SS = 0.76\%$, CCN is overestimated by ~5%. Different performance of the CCN closure test under different supersaturations may be a result of differing chemical properties of different aerosol sizes. However, the large uncertainties in the prediction of CCN at lower SS are mainly caused by the less accuracy in setting lower supersaturation in CCN counter, as well as more noise in the concentrations at relatively larger sizes. Since we combined the SMPS with CCN counter, the measured CCN number concentrations were accordingly from a particle dry size range of 10–600 nm, the missing particles for which $D_p > 600$ nm should not be one of the reason to cause the uncertainty in CCN prediction at lower supersaturations in this study. These results show that the PSD measured by the SMPS, combined with the bulk K_{chem} calculated from the chemical composition information from the ACSM, can provide good estimates of N_{CCN} at higher supersaturations. Information about size-resolved chemical composition is expected a better agreement and more accurate estimates of CCN

number concentrations. The closure results are not good at lower supersaturations. Improving the measurement accuracy at lower supersaturations may be important to the prediction of CCN.

4.4. Influence of NPF on CCN activity

To study the impact of NPF on CCN activity, two cases, one with an NPF event (24 August 2014) and another with a non-NPF event (4 August 2014), were selected for study. Simultaneously measured PSD, mass concentrations of organics, sulfate, nitrate, activation ratios, calculated K_{chem} and f_{44} were examined during the two events (Fig. 6).

During the NPF event, the PSD showed a “banana” shape representative of a typical NPF event. The NPF event spanned the period from 1000 LT to 1600 LT. The mass concentrations of sulfate and organics increased significantly (by a factor of 4.17 and 1.35, respectively) during the NPF event, indicating that particle growth may have been driven by the condensation of atmospheric sulfuric acid and volatile organics. Other field measurements have also demonstrated that sulfate and organics contribute to particle growth during an NPF event (Zhang et al., 2004b; Yue et al., 2011; Leng et al., 2014a; Minguillón et al., 2015). The evident spike in organic aerosol mass concentration prior to

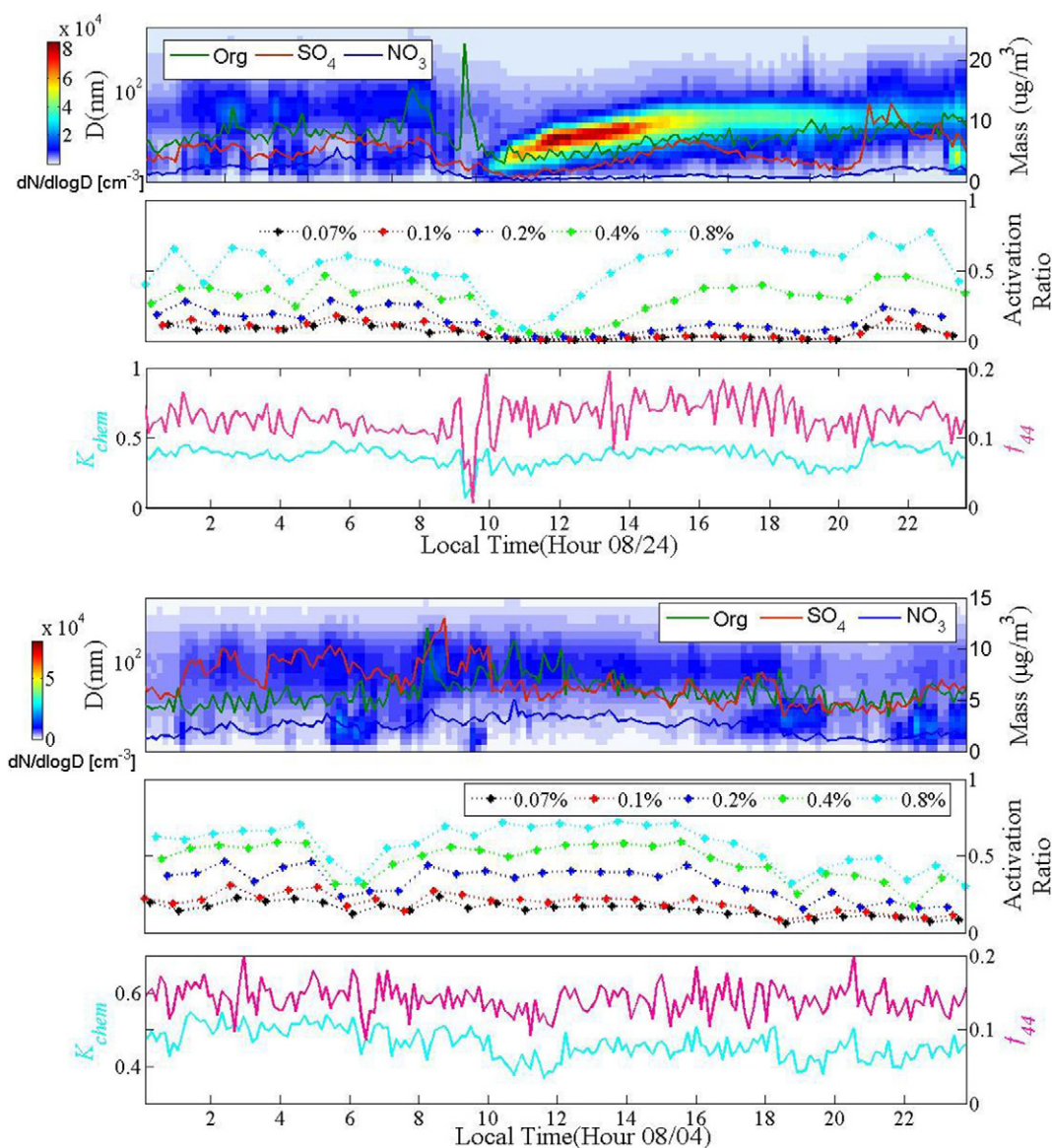


Fig. 6. Particle size distribution during the NPF event (top three panels, 24 August) and the non-NPF event (bottom three panels, 4 August). The color contour in the top panel of each figure denotes $dN/d\log D$ (cm⁻³) on the left vertical axis (where N and D represent the particle number and size, respectively).

10:00 AM may be due to a local impact from traffic sources (Wang et al., 2016). The mass concentration of nitrate observed at Xinzhou increased slightly during the period of 1000 LT to 1600 LT. Simultaneously, κ_{chem} and f_{44} showed a slight increase during the period of 1000 LT to 1600 LT, indicating that particles were becoming more hygroscopic and oxidative. More hygroscopic and oxidative particles are expected to activate more easily.

At the beginning of the NPF, a burst of nucleation mode occurs, resulted in a very large number of particles, however most of the particles sizes were smaller than the critical diameter, for example, critical diameter for pure $(\text{NH}_4)_2\text{SO}_4$ particles is 83 nm at SS of 0.17%, thus activation fraction showed a significant drop. AR started to increase as the nanoparticles grew larger between 1100 LT and 1600 LT. The increase in AR started 1 h after the burst of nucleation mode particles. Overall, the NPF event enhanced CCN activity, especially at higher SS (e.g., $\geq 0.17\%$). The impact was insignificant when the SS was low (e.g., $\leq 0.13\%$) due to the limitation of particle critical diameters. In this case, the increase in κ_{chem} and f_{44} suggests that the particles were more hygroscopic, which would favor particle growth during the NPF event and enhancement of the AR.

During the non-NPF event (4 August 2014), average mass concentrations of sulfate, nitrate, and organics were $5.8 \mu\text{g m}^{-3}$, $6.7 \mu\text{g m}^{-3}$, and $2.4 \mu\text{g m}^{-3}$, respectively. The calculated κ_{chem} and f_{44} changed slightly, suggesting an insignificant variation in particle hygroscopicity and oxidability. No “banana” shape was observed and accumulation-mode particles dominated all day long. The AR at all SS levels showed flat trends during the daytime. The AR decreased to <0.3 around 0600 LT and 1900 LT nucleation and accumulation mode peaks were seen in the PSD. The increase in small particles thus led to a reduction in AR.

To study the influence of the NPF event on CCN activation, simultaneous size-resolved CCN efficiency data measured during the periods of 1000–1200 LT and 1300–1500 LT, which were the key periods of

NPF, were selected for further investigation (Fig. 7). From 1000 to 1200 LT, the aerosol number concentrations in the NPF case were enhanced dramatically primarily in the nucleation and Aitken modes. We call this period the “growth” stage. From 1300 to 1500 LT, the particle size increased to ~ 100 nm and the particle number concentrations stopped increasing. We call this period the “leveling-off” stage. During the “growth” stage, the activation diameter (D_a) in the NPF case was on average larger than that observed during the non-NPF case. The increase in AR as D_a increased observed during the NPF event was more gradual. This suggests that during the “growth” stage, particles in the NPF case were more heterogeneous with less hygroscopicity, so were more difficult to activate. In other words, the NPF during the “growth” stage restrained CCN activation. During the “leveling-off” stage, however, the situation changed. The CCN efficiency spectra during the NPF event showed smaller D_a , steeper increases in AR as D_a increased. Therefore, the NPF during the “leveling-off” stage enhanced CCN activation. Based on our observations, NPF had different impacts on CCN activity at different times of the day during the NPF event. As shown in Fig. 7, the bulk AR from 1000 to 1200 LT was reduced during the NPF event, but began to increase after 1200 LT until reaching the accumulation mode size range.

5. Conclusions

In this study, we investigated the CCN activity and new particle formation impact on CCN activation based on the field campaign at the Xinzhou site in 2014. Both aerosol and CCN number concentrations were extremely high during the field campaign. The average bulk AR ranged from $12.6 \pm 8\%$ to $58.1 \pm 15\%$ for SS ranging from 0.075%–0.76%. We found that particle size was more related to the CCN activation ratios in the morning, whereas in the afternoon (~ 1400 LST), κ_{chem} and f_{44} were more closely associated with the bulk AR. Under the assumption of internal mixing, measured and predicted CCN

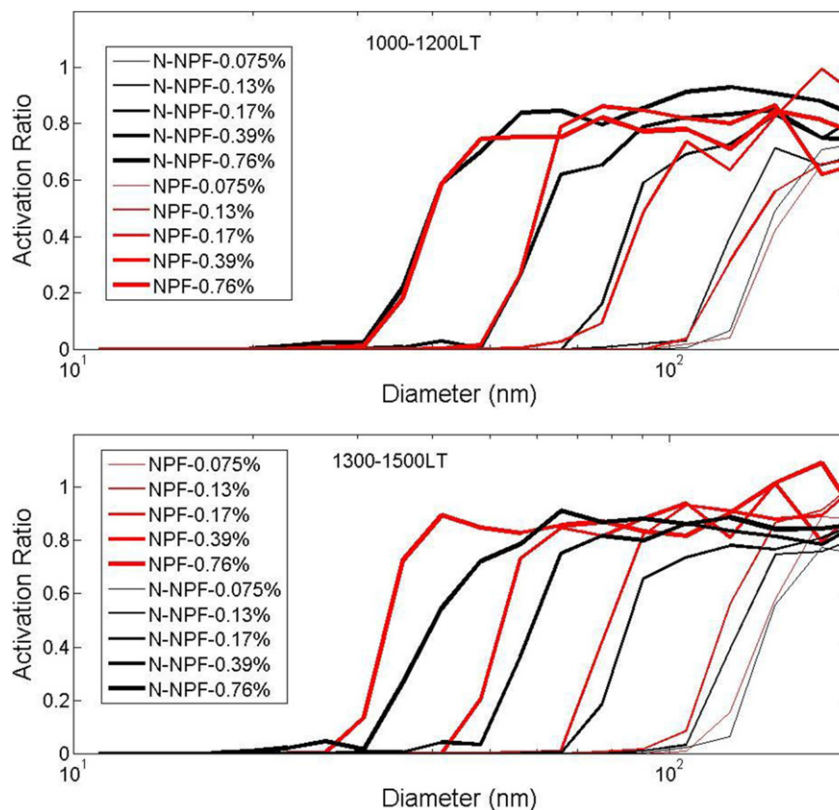


Fig. 7. Observed size-resolved CCN efficiency spectra for the NPF (red lines) and non-NPF cases (black lines) during the periods of 1000–1200 LT (top panel) and 1300–1500 LT (bottom panel). The different line thicknesses represent different SS levels.

number concentrations were compared using bulk chemical composition information based on κ -Köhler theory. We found that the predicted CCN number concentrations were underestimated by 20–30% at SS < 0.2% probably due to the measurement uncertainties. Estimates were more accurate at higher SS levels, suggesting that the hygroscopicity parameter based on bulk chemical composition information can provide a good estimate of CCN number concentrations. However, the size-resolved chemical composition is expected to improve the CCN number concentration prediction. The NPF showed a distinct effect on CCN activity at different periods. CCN activation was restrained at the “growth” stage, during which a larger size was required to reach the activation diameter, and accordingly bulk AR decreased by 500% at SS = 0.76%. CCN activation appeared to be enhanced during the “leveling-off” stage when the activation diameter was reduced and bulk AR began to increase quickly and was enhanced about 20% eventually. Our study showed that NPF events could either decrease or increase CCN number concentrations, as depends on their stage. According to our results, the effect or role of particles physiochemical properties on CCN activity largely depends on time of a day. In addition, it is important to classify the NPF events to at least two stages when evaluating the contribution of NPF to CCN number concentrations. Nevertheless, only one month data from one site is very limit to address the key issues in the research area and to parameterize CCN in models. Depending on the location, more field measurements and data are therefore necessary to validate the complex effect of particles properties on CCN activity, in particular in those heavily polluted regions.

Acknowledgements

This work was supported by NSCF research project (grant no. 41675141, 91544217, 41605109), the National Basic Research Program of China ‘973’ (grant no. 2013CB955800), and the NSCF-TAMU Collaborative Research Grant Program (grant no. 4141101031). We thank the Xinzhou Meteorological Administration for meteorological data from the field campaign used in this study. We also thank all participants in the field campaign at Xinzhou for their tireless work and co-operation.

References

- Albrecht, B.A., 1989. Aerosols, cloud microphysics, and fractional cloudiness. *Science* 245, 1227–1230.
- Almeida, G.P., Brito, J., Morales, C.A., Andrade, M.F., Artaxo, P., 2014. Measured and modelled cloud condensation nuclei (CCN) concentration in São Paulo, Brazil: the importance of aerosol size-resolved chemical composition on CCN concentration prediction. *Atmos. Chem. Phys.* 14 (14), 7559–7572.
- Andreae, M.O., Rosenfeld, D., 2008. Aerosol-cloud-precipitation interactions, part 1: the nature and sources of cloud-active aerosols. *Earth Sci. Rev.* 89, 13–41.
- Anttila, T., Kerminen, V.-M., 2007. On the contribution of Aitken mode particles to cloud droplet populations at continental background areas – a parametric sensitivity study. *Atmos. Chem. Phys.* 7:4625–4637. <http://dx.doi.org/10.5194/acp-7-4625-2007>.
- Asmi, E., Kivekäs, N., Kerminen, V.M., Komppula, M., Hyvärinen, A.P., Hatakka, J., Viisanen, Y., Lihavainen, H., 2011. Secondary new particle formation in Northern Finland Pallas site between the years 2000 and 2010. *Atmos. Chem. Phys.* 11 (24), 12959–12972.
- Birmili, W., Wiedensohler, A., 2000. New particle formation in the continental boundary layer: meteorological and gas phase parameter influence. *Geophys. Res. Lett.* 27: 3325–3328. <http://dx.doi.org/10.1029/1999GL011221>.
- Cheng, Y., Lee, S.C., Ho, K.F., Wang, Y.Q., Cao, J.J., Chow, J.C., Watson, J.G., 2006. Black carbon measurement in a coastal area of south China. *J. Geophys. Res. Atmos.* 111, D12310. <http://dx.doi.org/10.1029/2005JD006663>.
- Chin, M., Kahn, R.A., Schwartz, S.E. (Eds.), 2009. *Atmospheric Aerosol Properties and Climate Impacts. A Report by the U.S. Climate Change Science Program and the Subcommittee on Global Change Research.* National Aeronautics and Space Administration, Washington, D.C., USA.
- Dal Maso, M., Kulmala, M., Riipinen, I., Wagner, R., Hussein, T., Aalto, P.P., Lehtinen, K.E.J., 2005. Formation and growth of fresh atmospheric aerosols: eight years of aerosol size distribution data from SMEAR II, Hyytiälä, Finland. *Boreal Environ. Res.* 10, 323–336.
- DeFolice, T.P., Saxena, V.K., 1994. On the variation of cloud condensation nuclei in association with cloud systems at a mountain-top location. *Atmos. Res.* 31, 13–39.
- Deng, Z., Zhao, C., Ma, N., Liu, F., Ran, L., Xu, W., Liang, Z., Liang, S., Huang, M., Ma, X., Zhang, Q., Quan, J., Yan, P., 2011. Size-resolved and bulk activation properties of aerosols in the North China Plain. *Atmos. Chem. Phys.* 11, 3835–3846.
- Deng, Z., Zhao, C., Ma, N., Ran, L., Zhou, G., Lu, D., Zhou, X., 2013. An examination of parameterizations for the CCN number concentration based on in situ measurements of aerosol activation properties in the North China Plain. *Atmos. Chem. Phys.* 13: 6227–6237. <http://dx.doi.org/10.5194/acp-13-6227-2013>.
- Dumka, U.C., Krishna Moorthy, K., Kumar, R., Hegde, P., Sagar, R., Pant, P., Singh, N., Suresh Babu, S., 2010. Characteristics of aerosol black carbon mass concentration over a high altitude location in the Central Himalayas from multi-year measurements. *Atmos. Res.* 96, 510–521.
- Dusek, U., Frank, G.P., Hildebrandt, L., Curtius, J., Schneider, J., Walter, S., Chand, D., Drewnick, F., Hings, S., Jung, D., Borrmann, S., Andreae, M.O., 2006. Size matters more than chemistry for cloud-nucleating ability of aerosol particles. *Science* 312 (5778), 1375–1378.
- Gunthe, S.S., King, S.M., Rose, D., Chen, Q., Roldin, P., Farmer, D.K., Jimenez, J.L., Artaxo, P., Andreae, M.O., Martin, S.T., Pöschl, U., 2009. Cloud condensation nuclei in pristine tropical rainforest air of Amazonia: size-resolved measurements and modeling of atmospheric aerosol composition and CCN activity. *Atmos. Chem. Phys.* 9:7551–7575. <http://dx.doi.org/10.5194/acp-9-7551-2009>.
- Heintzenberg, J., Wehner, B., Birmili, W., 2007. How to find bananas in the atmospheric aerosols: new approach for analyzing atmospheric nucleation and growth events. *Tellus* 59B, 273–282.
- Hudson, J., 2007. Variability of the relationship between particle size and cloud-nucleating ability. *Geophys. Res. Lett.* 34, L08801. <http://dx.doi.org/10.1029/2006GL028850>.
- Intergovernmental Panel on Climate Change, 2013. *Climate Change 2013: The Physical Scientific Basis.* Cambridge Univ. Press, Cambridge, United Kingdom and New York, NY, USA.
- Kalkavouras, P., Bossioli, E., Bezantakos, S., Bougiatioti, A., Kalivitis, N., Stavroulas, I., Kouvarakis, G., Protonotariou, A.P., Dandou, A., Biskos, G., Mihalopoulos, N., Nenes, A., Tombrou, M., 2017. New particle formation in the southern Aegean Sea during the Etesians: importance for CCN production and cloud droplet number. *Atmos. Chem. Phys.* 17, 175–192.
- Kuang, C., McMurry, P.H., McCormick, A.V., 2009. Determination of cloud condensation nuclei production from measured new particle formation events. *Geophys. Res. Lett.* 36 (9). <http://dx.doi.org/10.1029/2009GL037584>.
- Kulmala, M., Petäjä, T., Nieminen, T., Sipilä, M., Manninen, H.E., Lehtipato, K., Dal Maso, M., Aalto, P.P., Junninen, H., Paasonen, P., Riipinen, I., Lehtinen, K.E., Laaksonen, A., Kerminen, V.M., 2012. Measurement of the nucleation of atmospheric aerosol particles. *Nat. Prod.* 7, 1651–1667.
- Larson, S.M., Cass, G.R., Hussey, K.J., Luce, F., 1988. Verification of image processing based on visibility models. *Environ. Sci. Technol.* 22 (6):629–637. <http://dx.doi.org/10.1021/es00171a003>.
- Lee, L.A., Carslaw, K.S., Pringle, K.J., Mann, G.W., 2012. Mapping the uncertainty in global CCN using emulation. *Atmos. Chem. Phys.* 12 (20), 9739–9751.
- Leng, C.P., Cheng, T.T., Chen, J.M., Zhang, R.J., Tao, J., Huang, G.H., Zha, S.P., Zhang, M.G., Fang, W., Li, X., Li, L., 2013. Measurements of surface cloud condensation nuclei and aerosol activity in downtown Shanghai. *Atmos. Environ.* 69, 354–361.
- Leng, C., Zhang, Q., Tao, J., Zhang, H., Zhang, D., Xu, C., Li, X., Kong, L., Cheng, T., Zhang, R., Yang, X., Chen, J., Qiao, L., Lou, S., Wang, H., Chen, C., 2014a. Impacts of new particle formation on aerosol cloud condensation nuclei (CCN) activity in Shanghai: case study. *Atmos. Chem. Phys.* 14:11353–11365. <http://dx.doi.org/10.5194/acp-14-11353-2014>.
- Leng, C., Zhang, Q., Zhang, D., Xu, C., Cheng, T., Zhang, R., Tao, J., Chen, J., Zha, S., Zhang, Y., Li, X., Kong, L., Gao, W., 2014b. Variations of cloud condensation nuclei (CCN) and aerosol activity during fog-haze episode: a case study from Shanghai. *Atmos. Chem. Phys.* 14 (22):12499–12512. <http://dx.doi.org/10.5194/acp-14-12499-2014>.
- Li, Z., Chen, H., Cribb, M., Dickerson, R., Holben, B., Li, C., Lu, D., Luo, Y., Maring, H., Shi, G., Tsay, S.-C., Wang, P., Wang, Y., Xia, X., Zheng, Y., Yuan, T., Zhao, F., 2007. Preface to special section on East Asian Studies of Tropospheric Aerosols: An International Regional Experiment (EAST-AIRE). *J. Geophys. Res. Atmos.* 112 (D22). <http://dx.doi.org/10.1029/2007JD008853>.
- Li, J., Yin, Y., Li, P., Li, Z., Li, R., Cribb, M., Dong, Z., Zhang, F., Li, J., Rem, G., Jin, L., Li, Y., 2015. Aircraft measurements of the vertical distribution and activation property of aerosol particles over the Loess Plateau in China. *Atmos. Res.* 155, 73–86.
- Ma, Y., Brooks, S.D., Vidaurre, G., Khalizov, A.F., Wang, L., 2013. Rapid modification of cloud-nucleating ability of aerosols by biogenic emissions. *Geophys. Res. Lett.* 40: 6293–6297. <http://dx.doi.org/10.1002/2013GL057895>.
- Ma, N., Zhao, C.S., Tao, J.C., Wu, Z.J., Kecorius, S., Wang, Z.B., Größl, J., Liu, H.J., Bian, Y.X., Kuang, Y., Teich, M., Spindler, G., Müller, K., van Pinxteren, D., Herrmann, H., Hu, M., Wiedensohler, A., 2016. Variation of CCN activity during new particle formation events in the North China Plain. *Atmos. Chem. Phys.* 16, 8593–8607.
- McFiggans, G., Artaxo, P., Baltensperger, U., Coe, H., Facchini, M.C., Feingold, G., Fuzzi, S., Gysel, M., Laaksonen, A., Lohmann, U., Mentel, T.F., Murphy, D.M., O’Dowd, C.D., Snider, J.R., Weingartner, E., 2006. The effect of physical and chemical aerosol properties on warm cloud droplet activation. *Atmos. Chem. Phys.* 6:2593–2649. <http://dx.doi.org/10.5194/acp-6-2593-2006>.
- Mei, F., Setyan, A., Zhang, Q., Wang, J., 2013. CCN activity of organic aerosols observed downwind of urban emissions during CARES. *Atmos. Chem. Phys.* 13, 12155–12169.
- Medina, J., Nenes, A., Sotiropoulou, R.-E.P., Cottrell, L.D., Ziemba, L.D., Beckman, P.J., Griffin, R.J., 2007. Cloud condensation nuclei closure during the International Consortium for Atmospheric Research on Transport and Transformation 2004 campaign: effects of size-resolved composition. *J. Geophys. Res. Atmos.* 112, D10531. <http://dx.doi.org/10.1029/2006JD007588>.
- Miao, Q., Zhang, Z., Li, Y., Qin, X., Xu, B., Yuan, Y., Gao, Z., 2015. Measurement of cloud condensation nuclei (CCN) and CCN closure at Mt. Huang based on hygroscopic growth factors and aerosol number-size distribution. *Atmos. Environ.* 113, 127–134.
- Mingüillón, M.C., Brines, M., Pérez, N., Reche, C., Pandolfi, M., Fonseca, A.S., Amato, F., Alastuey, A., Lyasota, A., Codina, B., Lee, H.-K., Eun, H.-R., Ahn, K.-H., Querol, R., 2015. New particle formation at ground level and in the vertical column over the Barcelona area. *Atmos. Res.* 164–165 (2015), 118–130.
- Moore, R., Nenes, A., Medina, J., 2010. Scanning mobility CCN analysis – a method for fast measurements of size resolved CCN distributions and activation kinetics. *Aerosp. Sci. Technol.* 44, 861–871.
- Ng, N.L., Herndon, S.C., Trimborn, A., Canagaratna, M.R., Croteau, P.L., Onasch, T.B., Sueper, D., Worsnop, D.R., Zhang, Q., Sun, Y.L., Jayne, J.T., 2011. An aerosol chemical speciation monitor (ACSM) for routine monitoring of the composition and mass concentrations of ambient aerosol. *Aerosol Sci. Technol.* 45, 770–784.

- O'Dowd, C.D., 2001. Biogenic coastal aerosol production and its influence on aerosol radiative properties. *J. Geophys. Res. Atmos.* 106 (D2), 1545–1549.
- Olofson, K.F.G., Andersson, P.U., Hallquist, M., Ljungström, E., Tang, L., Chen, D., Pettersson, J.B.C., 2009. Urban aerosol formation in the Arctic boundary layer. *J. Geophys. Res. Atmos.* 113, 8309–8321.
- Petters, M.D., Kreidenweis, S.M., 2007. A single parameter representation of hygroscopic growth and cloud condensation nucleus activity. *Atmos. Chem. Phys.* 7:1961–1971. <http://dx.doi.org/10.5194/acp-7-1961-2007>.
- Pringle, K.J., Tost, H., Pozzer, A., Pöschl, U., Lelieveld, J., 2010. Global distribution of the effective aerosol hygroscopicity parameter for CCN activation. *Atmos. Chem. Phys.* 10: 5241–5255. <http://dx.doi.org/10.5194/acp-10-5241-2010>.
- Quinn, P.K., Bates, T.S., Coffman, D.J., Covert, D.S., 2008. Influence of particle size and chemistry on the cloud nucleating properties of aerosols. *Atmos. Chem. Phys.* 8: 1029–1042. <http://dx.doi.org/10.5194/acp-8-1029-2008>.
- Rissman, T.A., VanReken, T.M., Wang, J., Gasparini, R., Collins, D.R., Jonsson, H.H., Brechtel, F.J., Flagan, R.C., Seinfeld, J.H., 2006. Characterization of ambient aerosol from measurements of cloud condensation nuclei during the 2003 Atmospheric Radiation Measurement Aerosol Intensive Observational Period at the Southern Great Plains site in Oklahoma. *J. Geophys. Res. Atmos.* 111, D05S11. <http://dx.doi.org/10.1029/2004JD005695>.
- Roberts, G.C., Nenes, A., 2006. A continuous-flow streamwise thermal-gradient CCN chamber for atmospheric measurements. *Aerosol Sci. Technol.* 39, 206–221.
- Rose, D., Gunthe, S.S., Mikhailov, E., Frank, G.P., Dusek, U., Andreae, M.O., Pöschl, U., 2008. Calibration and measurement uncertainties of a continuous-flow cloud condensation nuclei counter (DMT-CCNC): CCN activation of ammonium sulfate and sodium chloride aerosol particles in theory and experiment. *Atmos. Chem. Phys.* 8:1153–1179. <http://dx.doi.org/10.5194/acp-8-1153-2008>.
- Shen, X., Sum, J., Zhang, Y., Wehner, B., Nowak, A., Tuch, T., Zhang, X., Wang, T., Zhou, H., Zhang, X., 2011. First long-term study of particle number size distributions and new particle formation events of regional aerosol in the North China Plain. *Atmos. Chem. Phys.* 11 (4), 1565–1580.
- Shi, J.P., Evans, D.E., Khan, A.A., Harrison, R.M., 2001. Sources and concentrations of nanoparticles (10 nm in diameter) in the urban atmosphere. *Atmos. Environ.* 35, 1193–1202.
- Sihto, S.-L., Mikkilä, J., Vanhanen, J., Ehn, M., Liao, L., Lehtipalo, K., Aalto, P.P., Duplissy, J., Petäjä, T., Kerminen, V.-M., Boy, M., Kulmala, M., 2011. Seasonal variation of CCN concentrations and aerosol activation properties in boreal forest. *Atmos. Chem. Phys.* 11: 13269–13285. <http://dx.doi.org/10.5194/acp-11-13269-2011>.
- Sun, Y., Wang, Z., Dong, H., Yang, T., Li, J., Pan, X., Chen, P., Jayne, J.T., 2012. Characterization of summer organic and inorganic aerosols in Beijing, China with an aerosol chemical speciation monitor. *Atmos. Environ.* 51:250–259. <http://dx.doi.org/10.1016/j.atmosenv.2012.01.013>.
- Turpin, B.J., Lim, H.J., 2001. Species contributions to PM_{2.5} mass concentrations: revisiting common assumptions for estimating organic mass. *Aerosol Sci. Technol.* 35, 602–610.
- Twomey, S., 1977. The influence of pollution on the shortwave albedo of clouds. *J. Atmos. Sci.* 34, 1149–1152.
- Vakkari, V., Laakso, H., Kulmala, M., Laaksonen, A., Mabaso, D., Molefe, M., Kgabi, N., Laakso, L., 2011. New particle formation events in semi-clean South African savannah. *Atmos. Chem. Phys.* 11:3333–3346. <http://dx.doi.org/10.5194/acp-11-3333-2011>.
- Wang, Z.B., Hu, M., Sun, J.Y., Wu, Z.J., Yue, D.L., Shen, X.J., Zhang, Y.M., Pei, X.Y., Cheng, Y.F., Wiedensohler, A., 2013. Characteristics of regional new particle formation in urban and regional background environments in the North China Plain. *Atmos. Chem. Phys.* 13:12495–12506. <http://dx.doi.org/10.5194/acp-13-12495-2013>.
- Wang, Q., Zhao, J., Du, W., Ana, G., Wang, Z., Sun, L., Wang, Y., Zhang, F., Li, Z., Ye, X., Sun, Y., 2016. Characterization of submicron aerosols at a suburban site in central China. *Atmos. Environ.* 131, 115–123.
- Wiedensohler, A., Cheng, Y.F., Nowak, A., Wehner, B., Achtert, P., Berghof, M., Birmili, W., Wu, Z.J., Hu, M., Zhu, T., Takegawa, N., Kita, K., Kondo, Y., Lou, S.R., Hofzumahaus, A., Holland, F., Wahner, A., Gunthe, S.S., Rose, D., Su, H., Pöschl, U., 2009. Rapid aerosol particle growth and increase of cloud condensation nucleus activity by secondary aerosol formation and condensation: a case study for regional air pollution in north-eastern China. *J. Geophys. Res. Atmos.* 114, D00G08. <http://dx.doi.org/10.1029/2008JD010884>.
- Yu, F., Wang, Z., Luo, G., Turco, R., 2008. Ion-mediated nucleation as an important global source of tropospheric aerosols. *Atmos. Chem. Phys.* 8 (9), 2537–2554.
- Yue, D.L., Hu, M., Zhang, R.Y., Wu, Z.J., Su, H., Wang, Z.B., Peng, J.F., He, L.Y., Huang, X.F., Gong, Y.G., Wiedensohler, A., 2011. Potential contribution of new particle formation to cloud condensation nuclei in Beijing. *Atmos. Environ.* 45 (33), 6070–6077.
- Yum, S.S., James, G.H., 2004. Wintertime/summertime contrasts of cloud condensation nuclei and cloud microphysics over the South Ocean. *J. Geophys. Res.* 109, D06204. <http://dx.doi.org/10.1029/2003JD003864>.
- Zhang, Q., Stanier, C.O., Canagaratna, M.R., Jayne, J.T., Worsnop, D.R., Pandis, S.N., Jimenez, J.L., 2004b. Insights into the chemistry of new particle formation and growth events in Pittsburgh based on aerosol mass spectrometry. *Environ. Sci. Technol.* 38, 4797–4809.
- Zhang, Q., Meng, J., Quan, J., Gao, Y., Zhao, D., Chen, P., He, H., 2012. Impact of aerosol composition on cloud condensation nuclei activity. *Atmos. Chem. Phys.* 12:3783–3790. <http://dx.doi.org/10.5194/acp-12-3783-2012>.
- Zhang, F., Li, Y., Li, Z., Sun, L., Li, R., Zhao, C., Wang, P., Sun, Y., Liu, X., Li, J., Li, P., Ren, G., Fan, T., 2014. Aerosol hygroscopicity and cloud condensation nuclei activity during the AC3Exp campaign: implications for cloud condensation nuclei parameterization. *Atmos. Chem. Phys.* 14:13423–13437. <http://dx.doi.org/10.5194/acp-14-13423-2014>.
- Zhang, F., Li, Z., Li, Y., Sun, Y., Wang, Z., Li, P., Sun, L., Wang, P., Cribb, M., Zhao, C., Fan, T., Yang, X., Wang, Q., 2016. Impacts of organic aerosols and its oxidation level on CCN activity from measurement at a suburban site in China. *Atmos. Chem. Phys.* 16: 5413–5425. <http://dx.doi.org/10.5194/acp-16-5413-2016>.